

**Determination of Mn<sup>2+</sup> by a paper-based flexible electrochemical sensor**

**modified by NiFe<sub>2</sub>O<sub>4</sub> and CeO<sub>2</sub> nanoparticles**

Haonan Zhan <sup>a#</sup>, Jingxia Wang <sup>a#</sup>, Qiang Xue <sup>a\*</sup>, Yao Liu <sup>a</sup>, Zeyu Liu <sup>a</sup>, Haijiao Xie<sup>b</sup>,

Xiao Long <sup>c</sup>, Renzhe Bi <sup>c</sup>, Malini OLIVO <sup>c</sup>

<sup>a</sup> MOE Key Laboratory of Groundwater Circulation and Environmental Evolution,  
School of Water Resources and Environment, China University of Geosciences  
(Beijing), Beijing, 100083, PR China

<sup>b</sup> Hangzhou Yanqu Information Technology Co., Ltd., Hangzhou City, Zhejiang  
Province 310003, PR China

<sup>c</sup> A\*STAR Skin Research Labs (A\*SRL), Agency for Science, Technology and Research  
(A\*STAR), Nanos: 31 Biopolis Way, #07-01, Nanos, Singapore 138669, Republic of  
Singapore.

**\*Correspondence Author: Qiang Xue**

E-mail: [xueqiang@cugb.edu.cn](mailto:xueqiang@cugb.edu.cn)

<sup>#</sup> Indicates equal contribution.

## DFT Calculation Method

All of the first principle calculations were based on the Vienna Ab initio Simulation Package (VASP)<sup>1</sup>. The interaction between ions and valence electrons was described by Projected Augmented Wave (PAW)<sup>2</sup>, and the exchange-correlation interaction was described by the Perdew-Burke-Ernzerhof generalized gradient approximation (PBE-GGA)<sup>3, 4</sup>. The cut-off energy was set as 450 eV, and the convergence criteria for self-consistent electronic energy and residual force were respectively assumed to be  $10^{-4}$  eV/atom and 0.01 eV/Å, which could ensure sufficient accuracy. The k points are set  $2 \times 2 \times 1$  based on Monkhorst-Pack meshes for all systems.

Van der Waals (vdW) effects were considered in all structures and using the DFT-D3 correction method<sup>5</sup>. The calculated of all structures using the DFT + U method, the U value for Fe 3d, Ni 3d, Mn 3d and Ce 4f was set to 4.0 eV, 4.0 eV, 4.0 eV and 5.0 eV, the J value for Fe 3d, Ni 3d, Mn 3d and Ce 4f was set to 0.4 eV, 0.4 eV, 0.4 eV and 0.5 eV, respectively. The results of the density of states (DOS) were obtained by using the VASPKIT<sup>6</sup>. In addition, Bader charge was used to analyze the number of electron transfer<sup>7</sup>.

The equation for the adsorption energy ( $E_{\text{ads}}$ ) in this article is defined as:

$$E_{\text{ads}} = E_{X^*} - E_* - E_X$$

where  $E_{X^*}$ ,  $E_*$  and  $E_X$  is the energy of the total adsorbed system, substance and adsorbates, respectively.

To precisely define the working electrode area, an insulating film was cut using a cutting plotter (Teneth, Shenzhen, China). The procedure involves the following steps: First, a clean blue film is loaded into the cutting plotter, and the desired cutting pattern, dimensions, and quantity are configured via computer software. The machine is then activated to execute the cutting process, producing uniformly sized insulating films. These films are subsequently affixed to the prepared integrated LIG electrode. A detailed illustration of this preparation process is provided in **Fig. S1**.



**Fig. S1** The preparation to control reaction area of the integrated electrode.



**Fig. S2** The photographs of the LIG.

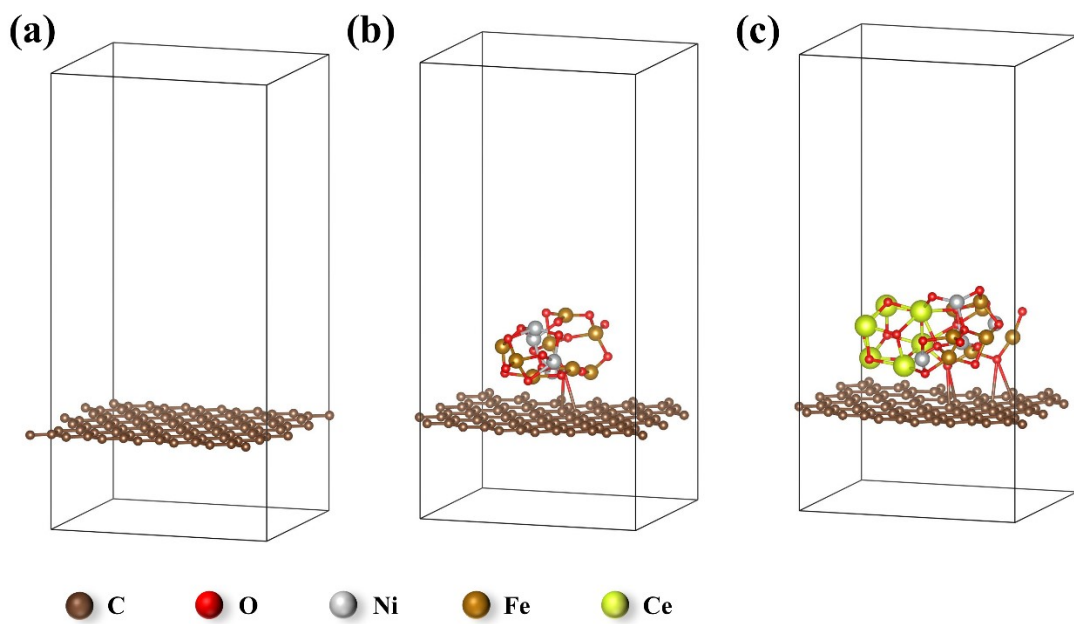


**Fig. S3** Calculation unit cell model of LIG (a),  $\text{NiFe}_2\text{O}_4/\text{LIG}$  (b),  $\text{NiFe}_2\text{O}_4/\text{CeO}_2/\text{LIG}$  (c).

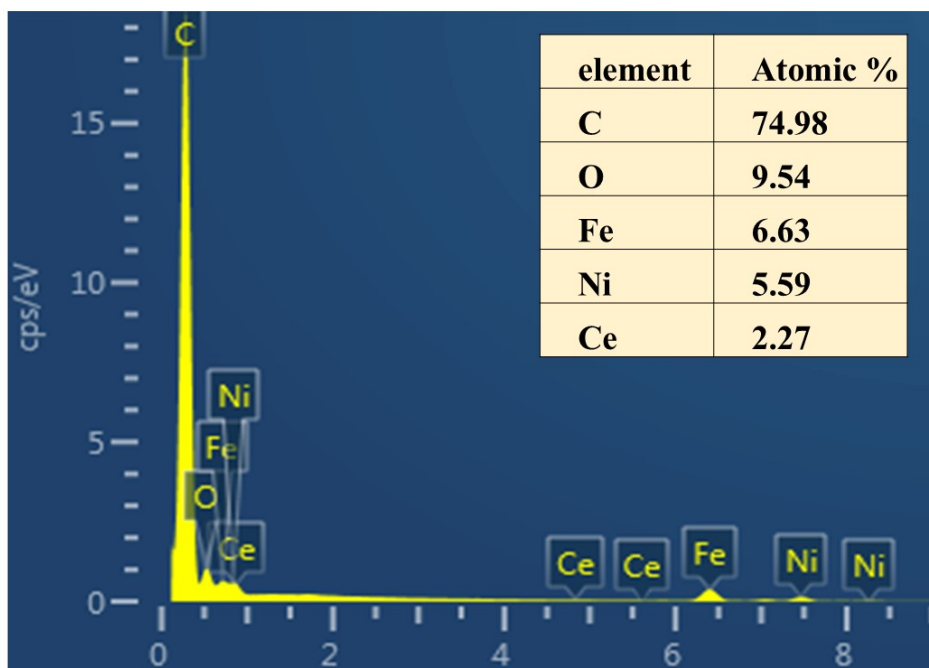


**Fig. S4** Total spectrum of the distribution mapping of NiFe<sub>2</sub>O<sub>4</sub>/CeO<sub>2</sub>/LIG (d).

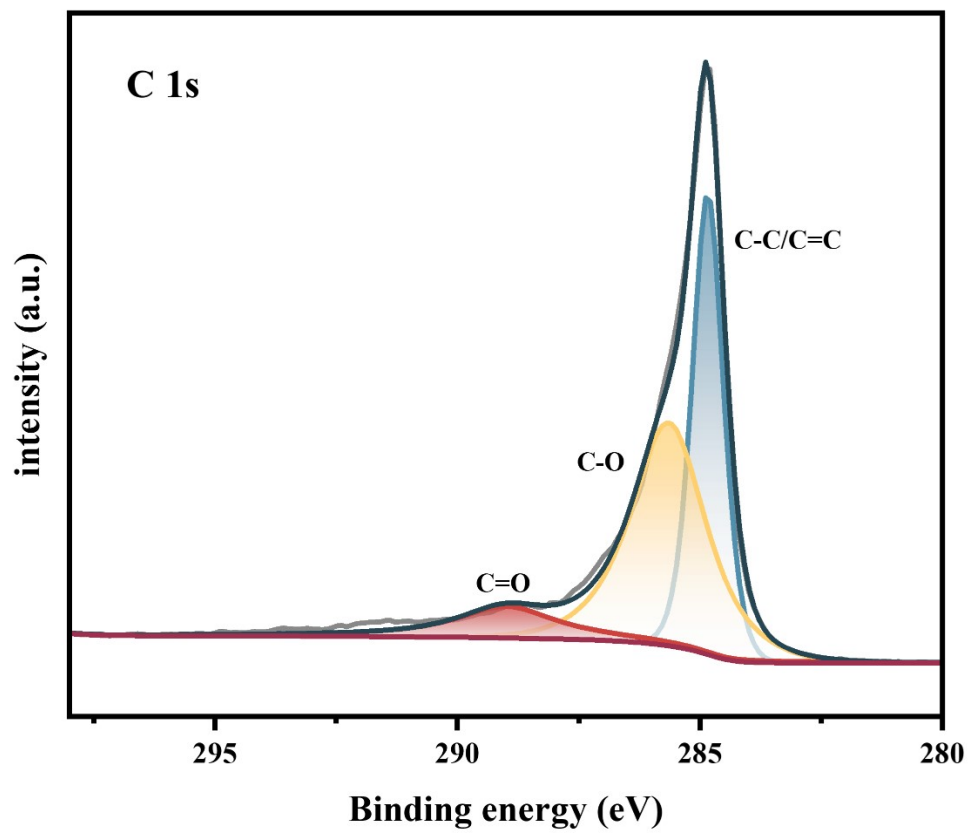


**Fig. S5** C 1s spectrum of NiFe<sub>2</sub>O<sub>4</sub> /LIG.

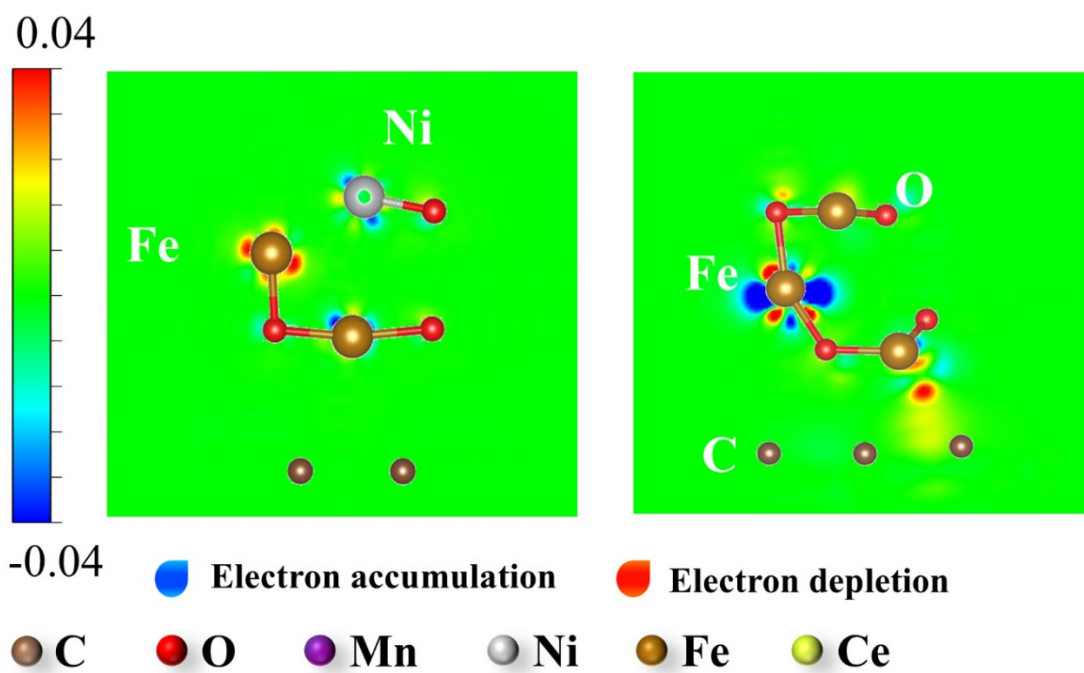


**Fig. S6** The two-dimensional slice plot of the Bader charge distribution of NiFe<sub>2</sub>O<sub>4</sub>/LIG.



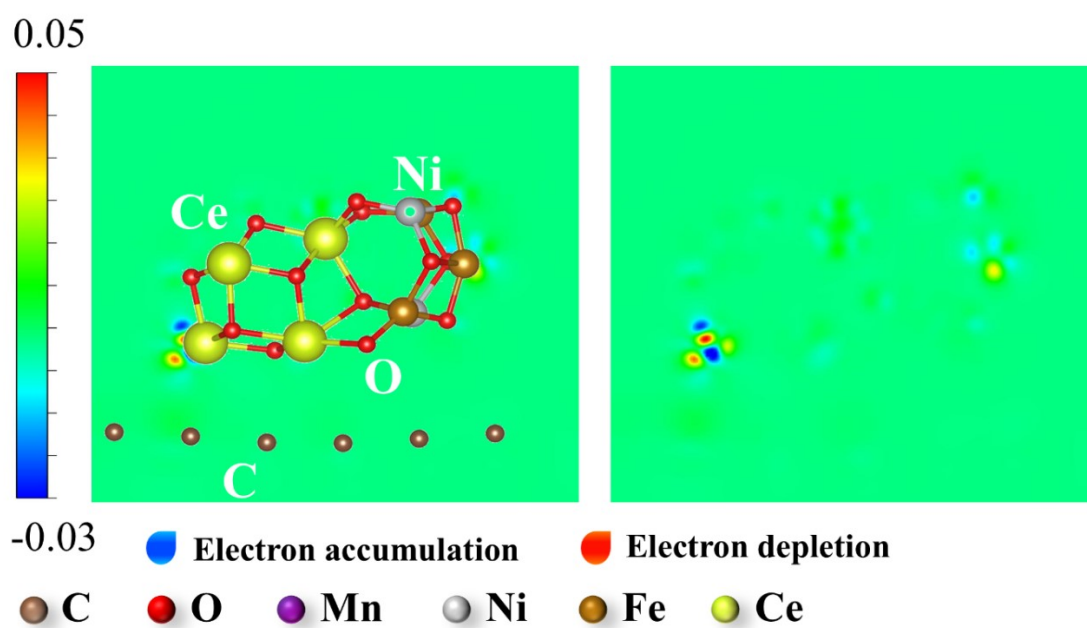


**Fig. S7** The two-dimensional slice plot of the Bader charge distribution of NiFe<sub>2</sub>O<sub>4</sub>/CeO<sub>2</sub>/LIG.

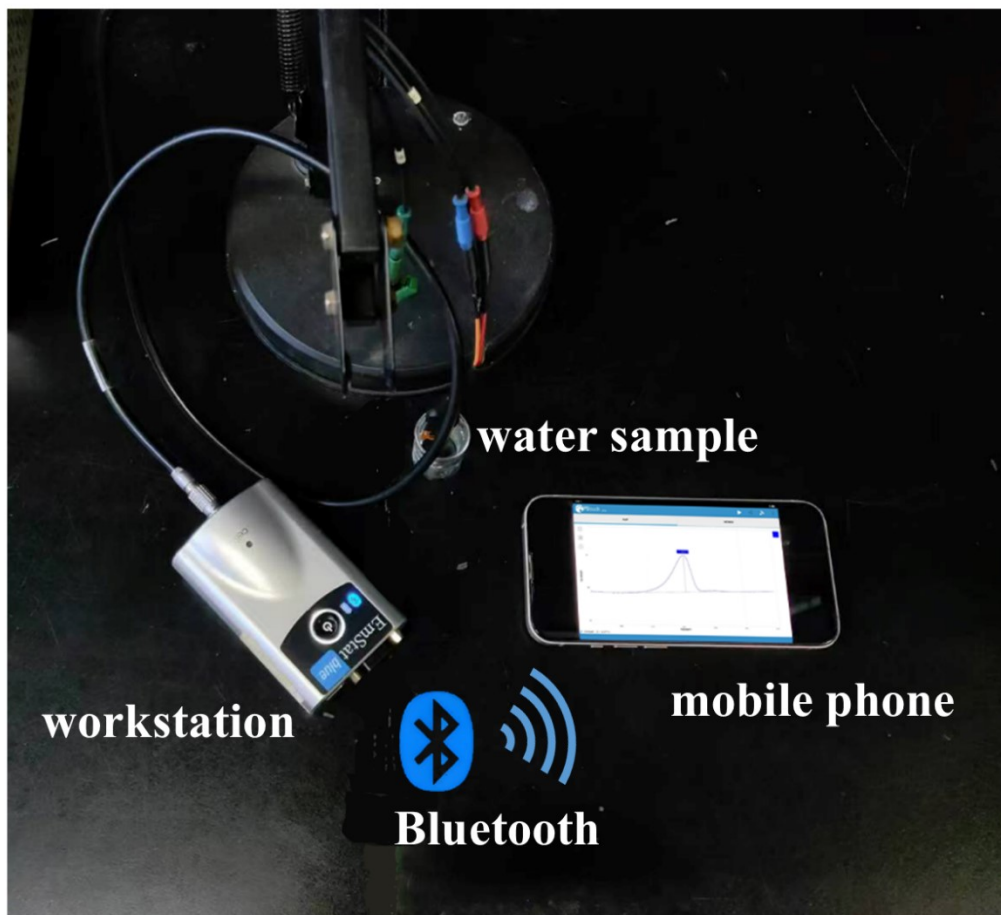


**Fig. S8** The equipment of actual detection.

**Table S1** Bader charge of each element and chemical in NiFe<sub>2</sub>O<sub>4</sub>/LIG.

elements	C	Fe	Ni	O
After reaction	287.747	54.077	36.160	110.016
Before reaction	288	64	40	96
Bader charge	-0.253	-9.923	-3.84	14.016
Total	C: -0.253		NiFe <sub>2</sub> O <sub>4</sub> : 0.253	

**Table S2** Bader charge of each element and chemical in NiFe<sub>2</sub>O<sub>4</sub>/CeO<sub>2</sub>/LIG.

elements	C	Fe	Ni	Ce	O <sub>2</sub>	O <sub>1</sub>
After reaction	288.072	54.843	36.755	59.147	36.621	120.559
Before reaction	288	64	40	72	36	96
Bader charge	0.072	-9.157	-3.245	-12.853	0.621	24.559
Total	C: 0.072	NiFe <sub>2</sub> O <sub>4</sub> :12.159		CeO <sub>2</sub> :12.232		

**Table S3** The BET specific surface areas of different electrodes

<b>Samples</b>	<b>S<sub>BET</sub> (m<sup>2</sup>·g<sup>-1</sup>)</b>
LIG	143.79
NiFe <sub>2</sub> O <sub>4</sub> /LIG	154.02
NiFe <sub>2</sub> O <sub>4</sub> /CeO <sub>2</sub> /LIG	217.15

**Table S4** Comparisons with standard methods.

Samples	Spiked concentration ( $\mu\text{g/L}$ )	Detected concentration ( $\mu\text{g/L}$ )	RSD (%)	Recycle (%)
Groundwater	100.00	122.37	2.22	118.18
	500.00	538.36	3.42	107.67
Tap water	100.00	98.60	8.14	98.60
	500.00	02.45	1.44	100.49

## Reference

1. G. Kresse and J. J. P. r. B. Furthmüller, 1996, **54**, 11169.
2. P. E. J. P. r. B. Blöchl, 1994, **50**, 17953.
3. J. P. Perdew, K. Burke and M. J. P. r. l. Ernzerhof, 1996, **77**, 3865.
4. J. P. Perdew, K. Burke and Y. J. P. r. B. Wang, 1996, **54**, 16533.
5. S. J. J. o. c. c. Grimme, 2006, **27**, 1787-1799.
6. V. Wang, N. Xu, J. Liu, G. Tang and W. G. J. D. h. d. o. j. c. VASPKIT, 2021, 108033.
7. W. Tang, E. Sanville and G. J. J. o. P. C. M. Henkelman, 2009, **21**, 084204.